

## Article

# Numerical Simulation of a New Designed Mechanical Seals with Spiral Groove Structures

Tao He <sup>1,2</sup>, Qiangqiang Zhang <sup>2</sup>, Ying Yan <sup>2,\*</sup> , Jintong Dong <sup>2</sup> and Ping Zhou <sup>2</sup> <sup>1</sup> Wuhan Second Ship Design and Research Institute, Wuhan 430205, China<sup>2</sup> Key Laboratory for Precision and Non-Traditional Machining Technology of Ministry of Education, Dalian University of Technology, Dalian 116024, China

\* Correspondence: yanying@dlut.edu.cn

**Abstract:** The spiral groove seal has a strong hydrodynamic effect, but it has poor pollution resistance at the seal's end and has unfavorable sealing stability. Circumferential waviness seals can use the fluid to clean the surface and have a strong ability to self-rush, protecting the main cover from contamination. This study presents a novel wave-tilt-dam seal design that integrates spiral groove structures to enhance the hydrodynamic performance of circumferential waviness seals. The objective of the research is to evaluate the mechanical effectiveness of this new design through simulation modeling, with a focus on the impact of structural parameters such as rotational speed and seal pressure on the hydrodynamic behavior under various operating conditions. The results of the study indicate that the new structure effectively improves the hydrodynamic performance of the liquid seal, resulting in a significant increase in film rigidity. Additionally, the study identifies optimal values for structural parameters under specific conditions. By addressing the limitations of traditional spiral groove seals and improving their hydrodynamic performance, this research contributes to the advancement of seal technology.

**Keywords:** mechanical seal; hydrodynamic effect; mechanical performance; spiral groove structures



**Citation:** He, T.; Zhang, Q.; Yan, Y.; Dong, J.; Zhou, P. Numerical Simulation of a New Designed Mechanical Seals with Spiral Groove Structures. *Lubricants* **2023**, *11*, 70. <https://doi.org/10.3390/lubricants11020070>

Received: 18 January 2023  
Revised: 5 February 2023  
Accepted: 7 February 2023  
Published: 9 February 2023



**Copyright:** © 2023 by the authors. Licensee MDPI, Basel, Switzerland. This article is an open access article distributed under the terms and conditions of the Creative Commons Attribution (CC BY) license (<https://creativecommons.org/licenses/by/4.0/>).

## 1. Introduction

Rotating machinery plays a significant role in the conversion or transmission of energy in the machinery industry. The issue of isolation and leakage from the outside world affects a lot of rotating equipment. The mechanical seal, acting as a dynamic sealing component, is widely used in all fields as an efficient means of resolving the leakage issue. Particularly in situations with difficult operating conditions, such as the sealing of reactor coolant pumps, it has emerged as the most efficient technique. The safety and dependability of equipment that uses mechanical seals as sealing components is directly impacted by the mechanical seals' performance. To enhance sealing performance, researchers create non-contacting seals for particular fields based on contacting seals. The introduction of micron-sized structure on the sealing surface between two seal rings allows the non-contacting seals to benefit from the hydrodynamic and hydrostatic effect of the process fluid.

The end surface structures that are commonly studied can be broadly divided into two categories based on the surface smoothness and the configuration of a single sealing ring cycle: slot structures and smooth surface structures. Within these categories, there are further distinctions between symmetrical and asymmetrical structures, each of which possess their own distinct performance characteristics. The textured structure is usually applied to one of the two sealing rings, while the other sealing ring typically features a smooth surface. Sealing rings made of harder materials, such as ceramics, possess good abrasion resistance and low wear rates, and are commonly used for micro-structural processing. Conversely, softer sealing rings, made of materials such as carbon graphite, have favorable lubrication properties and their surfaces are typically processed for smoothness.

The microstructures of mechanical and mechanical sealing tanks have been the subject of extensive research, with various structures such as straight grooves, curved grooves, and U-shaped groove structures having been applied in various fields, including aerospace, petro-chemical, and vehicle engineering. The groove structure is renowned for its good processing craftsmanship and ability to achieve required processing accuracy. In 1969, Cheng and Castelli introduced spiral grooves into the surface of mechanical seals, forming the initial spiral groove mechanical seal [1]. This structure has been found to have a higher bearing capacity and liquid film stiffness compared to other grooves, making it a classic structure in groove-type mechanical seals. Subsequently, research by Yuming Wang's group has examined the performance of the spiral groove seal under different lubrication conditions, such as oil membrane lubrication and gas lubrication [2,3]. Additionally, efforts have been made to optimize the structure parameters of a double spiral groove to improve sealing performance [4]. However, it has been noted that the groove structure may be deficient in some applications, particularly when dealing with process fluids containing impurities or crystallization. American engineer Pennink H highlighted this issue in his review of the 28 years of application of high-speed rotating equipment, citing the difficulty in ensuring the cleaning of the seal surface and the premature failure of the seal surface due to impurities particles and wear as problems faced by spiral grooves in such applications [5].

The smooth-surface seal is a distinct structural variant of end-surface seals, wherein the fluid static pressure is utilized as the primary means of achieving a seal. These seals typically feature a plane dam area on the low-pressure side, with the exterior surface extending to the high-pressure side being a cone, thus constituting the simplest form of smooth curved structure mechanical seal. The performance of these seals is dependent on the sealed pressure, thereby limiting their carrying capacity [6–8].

In 1989, Batch and INY introduced a radial seal that utilizes fluid dynamic pressure for lubrication, characterized by a smooth and weakly Wave-Tilt-Dam (WTD) surface on the sealing interface [9]. They examined the feasibility of this structure through experiments based on traditional fluid dynamic pressure theory and mechanics and found it to be viable. Subsequently, L.A. Young and A.O. Lebeck redesigned the component structure of the wave-shaped seal and conducted experiments to evaluate the performance of the oblique sealing structure, which showed to be exceptional [10]. In industrial applications, Lee S. validated the reliability of the mechanical seal in gas turbines to protect the turbine disk from hot combustion gases using the wave-shaped seal [11]. Additionally, Key B. and his team applied the wave-shaped seal to petroleum and natural gas pipelines, resulting in an increase in work life and reliability by overcoming the negative effects of particulate matter and process fluid changes on the sealing life [12]. The smooth curved surface allows for the self-flushing effect of the liquid film fluid on the seal surface, thereby maintaining the cleaning of the seal and avoiding the scratching effect of impurities particles on the seal surface, leading to improved stability of sealing performance. To further improve performance, researchers have used the structural parameters of the wave-cone-dam seal with the help of lubrication theory and experiments in different operating conditions [13–15]. Some combined structures and mutant structures are also proposed on the basis of the original structure, and its performance has begun to be studied and discussed [16,17]. Therefore, the proposal of new structures is of great significance in enhancing sealing and lubrication performance. However, different structures and sizes have distinct performance characteristics and scope of applications, and their performance requires further in-depth research and investigation.

Previous research has shown that while the spiral groove end-surface seal provides a strong hydrodynamic effect that improves performance, it also has a sensitivity to contaminants. Furthermore, the force curve of the axially movable ring, as depicted in Figure 1, demonstrates that cavitation has a significant impact on the fluid film's carrying capacity and stiffness. As the anti-vibration ability of the seal is dependent on the film stiffness, and the hydrodynamic pressure has the potential to provide sufficient force, a new type of mechanical seal, the SG-WTD seal, has been introduced to enhance the hydrodynamic

effect. A theoretical model has been developed to investigate the impact of three geometric parameters on the hydrodynamic seals, and numerical analysis has been conducted to evaluate the effects of these geometric changes.

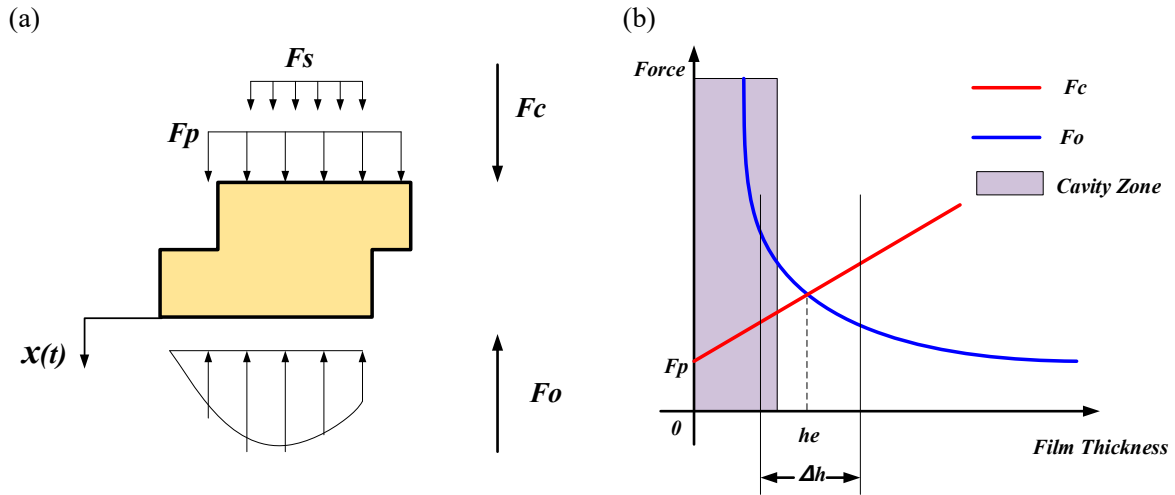


**Figure 1.** Force schematic of axially movable ring on WTD seal: (a) force diagram; (b) force curves. The symbols:  $F_p$ —back pressure,  $F_c$ —closing force,  $F_o$ —opening force,  $h_e$ —equilibrium film thickness,  $\Delta h$ —range of fluctuation of film thickness.

**2. Theory and Model**

**2.1. Geometry Model**

The mechanical sealing structure primarily consists of three components: a dynamic ring, a static ring, and a liquid film that is positioned between the two rings. The dynamic ring, which is attached to the rotating shaft, rotates during operation and impels the viscous fluid to flow in a circumferential direction. The fluid velocity is assumed to be uniform in a layer near the dynamic ring and gradually decreases as the distance from the dynamic ring increases, until it reaches the static ring. The fluid membrane that is confined by the sealing ring is the primary focus of research in fluid dynamic pressure mechanical seals, as depicted in Figure 2.

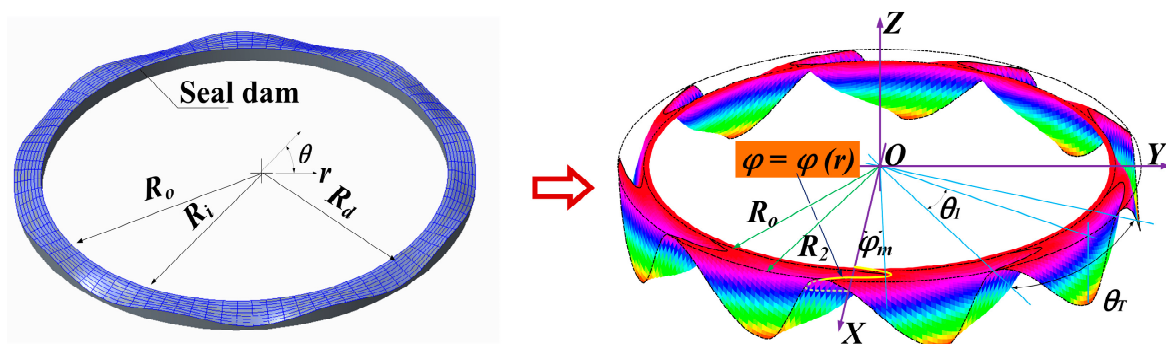


**Figure 2.** Schematic of wavy-tilt-dam mechanical seals with spiral groove structures (SG-WTD).

The end surface structure of the high-voltage internal flow-oriented internal flow-directional wavelet-type mechanical seal is a straight line with a specific taper on the flat inside of the cover surface and its inclination angle along the ripples of the regular changes of the string of the string. The expression of the end facial mask with a single cycle of the wave-type mechanical seal in column coordinates is:

$$h = \begin{cases} h_0 + t \cdot \Delta r \cdot y, & r > R_d \\ h_0, & r < R_d \end{cases} \tag{1}$$

where  $h$  is the coordinates of the thick direction of the membrane thickness on the sealing rings,  $h_0$  is the minimum liquid film thickness,  $h_t$  is the height of the outer diameter of the equivalent cone,  $h_a$  is the amplitude of the string waves at the outer diameter of the sealed outer diameter,  $R_d$  is the outer diameter of the dam area, the  $R_i$  is the inner diameter of the sealing ring,  $R_o$  is the outer diameter of the sealing ring,  $\alpha$  is the ratio of the high volatility and the high-end cone height,  $n$  is the number of waves, and  $\theta$  is the angle coordinate of any point.  $R_0$  to  $R_2$  is the analytical smooth surface section adjacent to the high-pressure boundary at  $R_2$ . It clearly consists of a Wavy-Tilt surface with a trough orientation that is governed by the function  $\varphi_0(r)$ , with radial coordinate acting as the independent variable. Actually, the function,  $\varphi_0(r)$ , defines changing initial phase along radial direction which determines angle offset value of circumferential cosine wave relative to the zero-angle radial line depending on radial coordinate. The phrase is given as follows,

$$\varphi_0 = \varphi_m \cdot \sin \left[ \frac{2\lambda\pi}{r_2 - r_0} (r - r_0) \right] \quad (2)$$

$$\varphi_m = \beta \cdot \theta_T \quad (3)$$

where  $r_2$  equals to  $R_2$ ,  $r_0$  is the same with  $R_0$ ,  $\theta_T$  is the minimum circumferential period in angle direction, and  $r$  is the local radial coordinate. According to the aforementioned investigations, convergent zones also affect the effect of hydrodynamic pressure lifting, and divergent zones have an impact on the level of liquid cavitation. The earlier arrangement prevented two zones from utilizing the same angle space. However, the restriction is lifted in order to obtain more comprehensive results. The parameter  $\alpha$  which represents the divergence area proportion is the ratio of divergent angle  $\theta_1$  to periodic angle  $\theta_T$ . The following form can be used to express the formula:

$$\alpha = \frac{\theta_1}{\theta_T} \quad (4)$$

The other two coefficients,  $\beta$  controls maximum value  $\varphi_m$  of initial phase offset,  $\lambda$  determines the shape of sinusoidal pattern selected in this article between  $R_0$  and  $R_2$ , as shown in Figure 2. Finally, a new face surface with three parameters  $\alpha$ ,  $\beta$ ,  $\lambda$  is established. The parameter  $\beta$  controls both the magnitude of the phase offset value and the angle of the valley. If the parameter  $\beta = 0$ , and  $\alpha = 0.5$ , the structure is the WTD type. When  $\beta$  is greater than zero, the high lines such as the structure will form a convergent depression along the direction of fluid flow.

For the SG-WTD surface, the local film thickness,  $h(r, \theta)$ , is given by:

$$h(r, \theta) = \begin{cases} h_0 + slope \cdot (r - r_0) \cdot (1 - \gamma \cdot y), & r > r_0 \\ h_0, & r < r_0 \end{cases} \quad (5)$$

where  $slope$  is the taper on the ring face,  $\gamma$  is ratio of wave amplitude and height of the taper at outer radius. The parameter  $y$  is the intermediate variable which symbolizes the shape of the circumferential curve in the cylinder at certain radius. It is also a function including independent variable of angle coordinate  $\theta$ , and a controlling parameter  $r$ . The equation is expressed as follows,

$$y(\theta) = \begin{cases} \cos \left[ \frac{n}{2\alpha} (\theta - \varphi_0) \right], & \theta \in \left[ 0, \frac{2\pi}{n} \right] \\ \cos \left[ \frac{n}{2(1-\alpha)} (\theta - \frac{2\pi}{n} - \varphi_0) \right], & \theta \in \left[ \frac{2\pi}{n}\alpha, \frac{2\pi}{n} \right] \end{cases} \quad (6)$$

where,  $n$  represents the number of angle periods,  $\theta$  is the local angle coordinate.

## 2.2. Kinematic Model

The equation which describes the pressure distribution of a lubricant film is the famous Reynolds equation, firstly presented in a landmark paper of Osborne Reynolds in 1886 [18]. The formula illustrated is as follows,

$$\nabla \cdot \left( \frac{\rho h^3}{12\mu} \nabla P \right) = \nabla \cdot (\vec{v} \rho h) + \frac{\partial(\rho h)}{\partial t} \quad (7)$$

where  $\nabla$  equals to  $\left( \frac{\partial}{\partial x}, \frac{\partial}{\partial y} \right)$ ,  $h$  is the film thickness,  $P$  is the local pressure,  $\mu$  is the liquid dynamic viscosity,  $\rho$  is the density of liquid,  $\vec{v}$  is the local velocity vector of different coordinate point, and  $t$  represents the physical parameter of time [18].

The boundary conditions include the inlet pressure  $P_o$  and the outlet pressure  $P_i$ , as shown by Equation (8). In addition, the paper also introduces the periodic condition, shown as Equation (9), in order to reduce the computational complexity.

$$P(R_i, \theta) = P_i, P(R_o, \theta) = P_o \quad (8)$$

$$P(r, 0) = P_i, P(r, \frac{2\pi}{n}) \quad (9)$$

In terms of research published in thrust bearings and mechanical seals studies, the JFO boundary condition provides more accurate simulation result, compared with other cavitation boundary conditions, due to consider the impact of mass conservation law when cavitation occurs [19]. Consequently, the JFO cavitation boundary condition, first reported by Jacobsson, Floberg, and Olsson [20–22], is used in order to achieve accurate leakage result which is a key parameter for evaluating the mechanical performance of the face seals designed. The Reynolds equation is solved by a finite element method [23,24].

The performance parameters used to evaluate the face seals include opening force, film stiffness, leakage and cavitation area. Each physical quantity is calculated by the following formula [14].

Opening force,

$$F_0 = \int_0^{2\pi} \int_{R_i}^{R_o} P \cdot r dr d\theta \quad (10)$$

Film stiffness,

$$K = -\frac{\partial F_0}{\partial h} \quad (11)$$

Leakage,

$$Q = \int_0^{2\pi} \int_0^h r \cdot V_r dz d\theta \quad (12)$$

The variable  $V_r$  is the radial component of speed vector  $\vec{v}$ .

Cavitation area,

$$S = \sum_{k=1}^N S_c(P = P_c) \quad (13)$$

The symbol  $N$  represents the number of grid cells, and  $S_c$  is the area of cell with cavitation.

## 2.3. Finite Element Method

The finite element method (FEM) was applied in this work. Method of normalization in the finite element method can enhance the resolution of the system of equations generated by the method, mitigate the influence of errors in the solution on the final outcome, and notably augment the precision of the solution. The expression of the normalization parameters is as follows,

$$H = \frac{h}{h_0}, P = \frac{p}{p_o}, X = \frac{r}{R_o}, Y = \frac{y}{R_o}, U_0 = \frac{u_0}{R_o}, V_0 = \frac{v_0}{R_o}, \bar{\rho} = \frac{\rho}{\rho_0} \quad (14)$$

And the governing equation can be obtained as follows,

$$\frac{\partial}{\partial X}(H^3 \frac{\partial P}{\partial X}) + \frac{\partial}{\partial Y}(H^3 \frac{\partial P}{\partial Y}) = \Lambda [\frac{\partial(U_0 \bar{\rho} H)}{\partial X} + \frac{\partial(V_0 \bar{\rho} H)}{\partial Y} + 2H \frac{\partial \bar{\rho}}{\partial t}] \quad (15)$$

It seeks to solve differential equations through the transformation of the equations into linear form through the application of advanced mathematical computation and manipulation. This is achieved by utilizing the method of separation of variables to obtain the division equation of the original problem [25],

$$\int_{\Omega} R \cdot \delta P dX dY = 0 \quad (16)$$

where  $\Omega$  represents the integral area,  $R$  represents the residual difference after the value of any value pressure is brought into the differential equation, and its expression is [14,26],

$$e = \frac{\partial}{\partial X}(H^3 \frac{\partial \bar{P}}{\partial X}) + \frac{\partial}{\partial Y}(H^3 \frac{\partial \bar{P}}{\partial Y}) - \Lambda [\frac{\partial(U_0 \bar{\rho} H)}{\partial X} + \frac{\partial(V_0 \bar{\rho} H)}{\partial Y} + 2H \frac{\partial \bar{\rho}}{\partial t}] \quad (17)$$

The general solution obtained from the underlying microcontroller equation, is generally not exact, resulting in a non-zero residual error  $e$ .

The forced boundary conditions of the lubrication model for mechanical seals are composed of inlet pressure ( $P_o$ ) and outlet pressure ( $P_i$ ). The value of the inlet pressure is equal to the pressure of the sealed process fluid. In this case, the values of different pressures are absolute pressures, and their expression is as follows,

$$\begin{cases} p(R_i, \theta) = p_i \\ p(R_o, \theta) = p_o \end{cases} \quad (18)$$

The incorporation of periodic boundary conditions, given the cyclical distribution of the sealing surface structure along the circumferential direction, can greatly simplify the number of nodes in the model, thereby reducing the computational scale of the program by a significant factor, as illustrated in Figure 2. Furthermore, if the periodicity of the microstructure of the seal ring along the circumferential direction is represented by  $n$ , the periodic boundary condition can be formulated as,

$$p(r, 0) = p(r, \frac{2\pi}{n}) \quad (19)$$

where  $r = \sqrt{x^2 + y^2}$  is the radius coordinate of any point.

In this study, the JFO boundary conditions are employed to arrive at a solution for the model. Despite the relative intricacy of the method for implementing JFO boundary conditions, it adheres to the fundamental principle of mass conservation, resulting in a higher level of confidence in the predicted leakage. Furthermore, the model established through the utilization of JFO boundary conditions also allows for the simultaneous forecasting of the load-bearing capacity, rigidity, distribution of liquid-gas mixture density, and area of cavitation in mechanical seals.

In order to simulate the cavitation process, the mixed density of the fluid is treated as a variable and the pressure of nodes below the cavitation pressure  $P_c$  is reset to that pressure during each iteration. Additionally, the dimensionless mixed density of the fluid is constrained to remain within the range of 0 to 1. Through repeated iterations, the pressure field will converge to a stable distribution, which represents the desired outcome. The criteria for determining the occurrence of cavitation within the iteration process assumes that the density of bubbles is 0 and the density of the non-cavitated liquid film is 1. The

judgment criterion for the cavitation boundary condition iteration process can be written as follows,

$$\begin{aligned} P &< P_c, P = P_c; \\ \bar{\rho} &< 0, \bar{\rho} = 0; \\ \bar{\rho} &> 1, \bar{\rho} = 1; \end{aligned} \quad (20)$$

Through iterative processes, the node pressure lower than the cavitation pressure  $P_c$  is reset to the empty pressure, and the mixing density of the fluid at the outer boundary is constrained to the range of 0 to 1, simulating the process of vacuuming. Through repeated iterations, the flow field will converge to a stable pressure distribution, which is the desired outcome. The liquid film that seals the mechanical seal is a crucial factor that determines its performance. Based on the numerical solution results obtained through the limited unit method, the main performance parameters of the mechanical seal can be evaluated. The computations are performed using the MATLAB programming platform and a liquid film computing program is developed, utilizing the JFO boundary condition with consideration for the conservation of fluid mass.

### 3. Results and Discussions

#### 3.1. Pressure Distribution

The shape and main data of the SG-WTD face mechanical seals used for the analysis are shown in Table 1. The pressure distributions along the mean diameter of single angle period  $\theta_T$  was analyzed in Figure 3. There were two kinds of lines in the figure. One was represented by the dotted curves belong to WTD seal, and the other was given by the solid curves reflecting the effect of SG-WTD seal. The parameter  $\beta$  which determines the magnitude of phase shifting will significantly influence the orientation of trough relative to radial direction. While this coefficient equals to zero, it means that the trend of line produced through linking extreme points in the mating ring face is in parallel with radial direction.

**Table 1.** Specification of SG-WTD seal face.

Item	Symbol	Dimensions and Data
Outside radius	$r_o$	50.1 mm
Inside radius	$r_i$	39.1 mm
Dam radius	$r_d$	41.1 mm
Number of periods	$n$	9
Tilt	<i>slope</i>	100 $\mu$ rad
Minimum film thickness	$h_0$	2 $\mu$ m
Amplitude coefficient of wave	$\gamma$	1

Figure 3a showed the comparison of pressure fields generated by two types of seals at various rotation speeds. According to the results, the hydrodynamic effect of SG-WTD seal was stronger than that of WTD. The SG-WTD seals had obvious advantages to obtain higher hydrodynamic pressure because of smaller cavitation area and larger maximum pressure contributing to improve opening force and film stiffness when they were operated at the same revolving speed. In addition, rotation speed had obviously a positive impact on peak values of liquid pressure, though lower profile appears in the cavitation zone. The effect of changing  $\beta$  on physical field mentioned above at the same rotation speed is presented in Figure 3b. Although the pressure in the pressurization district was weakened as the ratio raised, the cavitation level decreased simultaneously. According to the results, the higher cavitation area had a negative impact on bearing capacity, and stronger pressurization was the main factor to improve the bearing capacity. In general, the impact of cavitation and pressurization on sealing performance was opposite. An optimized value of  $\beta$  could be obtained for the best mechanical performance.

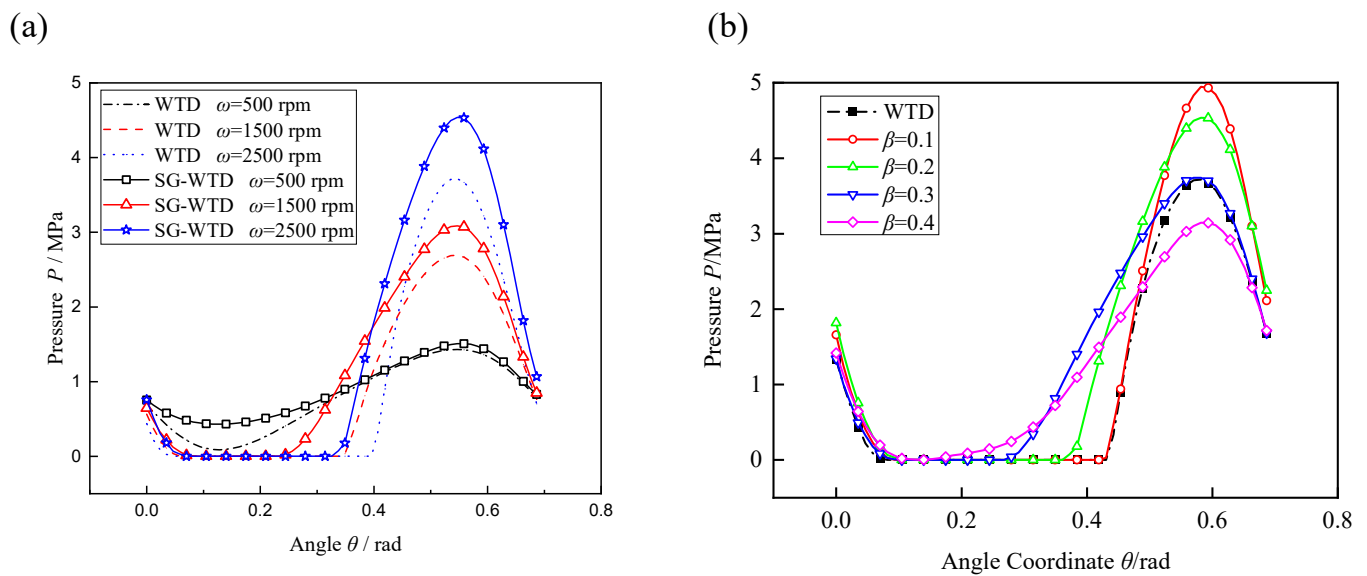


**Figure 3.** Pressure distribution along the mean diameter in single period, (a)  $\alpha = 0.7$ ,  $\beta = 0.2$ ,  $\lambda = 0.7$ ,  $P_o = 1.1$  MPa, (b)  $\alpha = 0.7$ ,  $\lambda = 0.7$ ,  $\omega = 1500$  rpm,  $P_o = 1.1$  MPa.

### 3.2. Influence of Operation Parameters

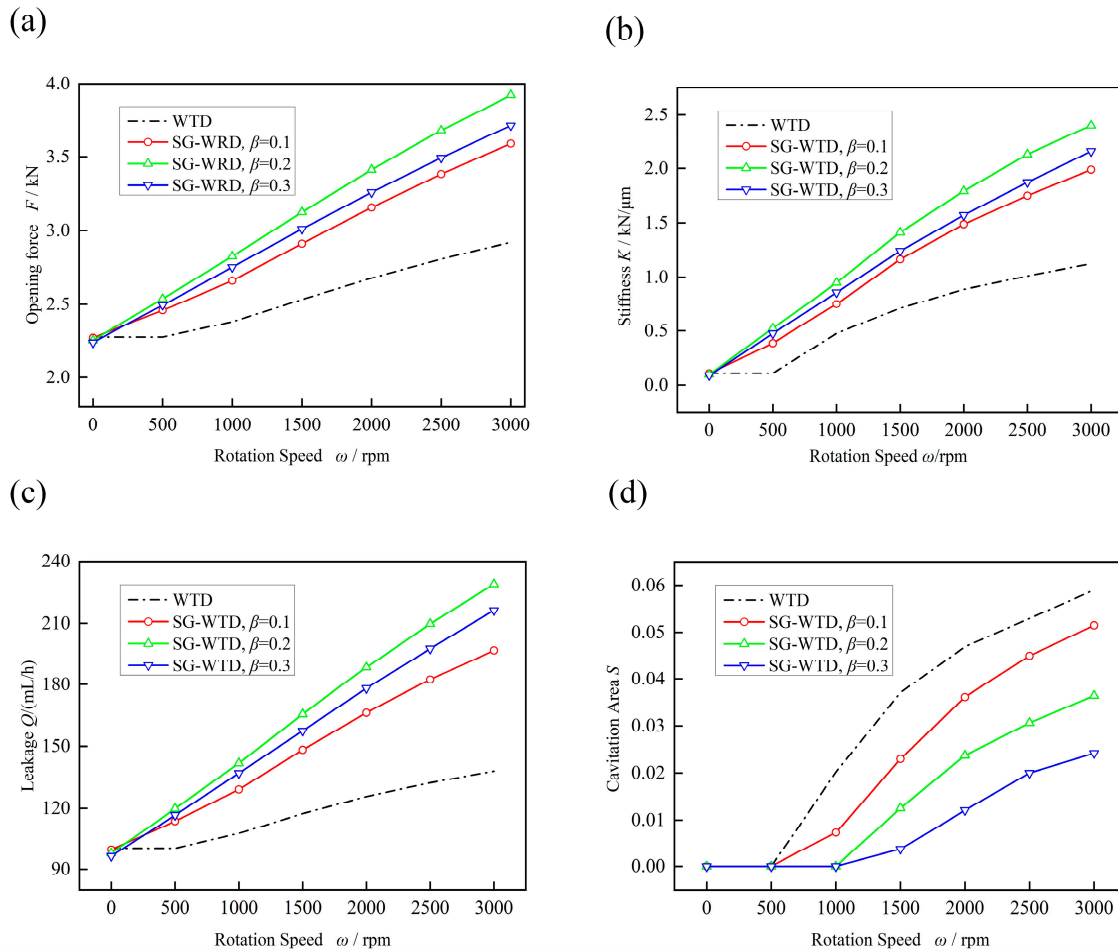
#### 3.2.1. Influence of Rotation Speed

Figure 4 illustrates the influence of rotation speed on the mechanical performance of the seal. The results of the study indicate that there is a critical point at  $\omega = 500$  rpm in the curves of opening force, rigidity, leakage, and cavitation. The cavitation effect was not observed at rotation speeds below 500 rpm, however, the pressurization trends varied. It was found that the SG-WTD structures, with respect to the three parameters that were used to measure the properties of the structure (bearing capacity, film rigidity, and leakage), remained relatively unchanged with an increase in rotation speed. As the rotation speed exceeded 500 rpm, the curves for the WTD seal also began to show an upward trend. It is reasonable to suggest that the hydrodynamic effect of the WTD seal may be closely related to the level of cavitation, as the appearance of cavitation and improvement in performance were observed simultaneously. Cavitation bubbles effectively prevent the pressure drop in the divergent zone to increase the opening force. As shown in Figure 4d, it was no doubt that the coefficient  $\beta$  drawn into the SG-WTD seal weakens the cavitation effect, which would contribute to improve bearing capacity. However, cavitation area correlated negatively with ratio  $\beta$ , while pressure peak value correlated positively with it. Therefore, the best value, i.e.,  $\beta = 0.2$ , existed between the other two values when performance values of three different were compared to one another. Finally, the leakage presented the similar trend as opening force and film stiffness.

#### 3.2.2. Influence of Seal Pressure

Figure 5 illustrates the impact of external diameter pressure on sealing performance at different  $\beta$  values. As shown in Figure 5a,c, the changing trends of load capacity and leakage flow are similar, with an increase in seal pressure leading to an increase in both. The differences between the curves are not significant. Figure 5b demonstrates the trend of rigidity of the liquid membrane, which differs significantly from the trend of bearing capacity and leakage volume. When the  $\beta$  value is very small, the high-end bending characteristics of the end surface structure are not pronounced, and the angle between the baseline of the valley and the radial line becomes very small. The stiffness curve for  $\beta = 0.1$  and the WTD structure shows a decline within a certain pressure range as the pressure of the outer diameter increases, but the degree of decline varies. Although the stiffness curves for  $\beta = 0.2$  and  $\beta = 0.3$  exhibit a growth trend, after a certain pressure value is exceeded, the growth rate of stiffness decreases significantly. Therefore, as the external

diameter pressure increases, the growth trend of rigidity of the liquid film is weakened. As the external diameter pressure continues to increase, the stiffness value for  $\beta = 0.1$  and the WTD structure begins to increase at a stable growth rate.



**Figure 4.** Influence of rotation speed on main mechanical performance ( $\alpha = 0.7$ ,  $\lambda = 0.7$ ,  $P_o = 1.1$  MPa), (a) opening force, (b) stiffness, (c) leakage, (d) cavitation.

For further study, the stiffness of statics and dynamics were investigated and the results were presented in Figure 6. Figure 6a shows that the hydrostatic opening forces increase with increasing sealing pressure even when the rotation speeds are artificially adjusted to zero. The WTD seal produced higher hydrostatic pressure than that of GS-WTD seal. The pressure decreased with the increase of  $\beta$ , and the differences between any two lines were further enlarged as  $P_o$  increased. The WTD seal created more hydrostatic pressure than the GS-WTD seal. The pressure decreased as  $P_o$  grew, and the disparities between any two lines widened. In terms of existing studies, total film pressure equals to the sum of the hydrodynamic pressure and hydrostatic pressure which is equivalent to pressure at  $\omega = 0$ . Figure 6b presents the curves of hydrodynamic stiffness  $\Delta K$  generated by subtracting hydrostatic stiffness  $K_0$  from total stiffness  $K$  shown in Figure 5b, which was expressed as Equation (21). The WTD and  $\beta = 0.1$  lines declined at  $P_o = 1.1$  MPa, and the lowering rates of cavitation areas became slow. Meanwhile, the other two lines of  $\beta = 0.2$  and  $\beta = 0.3$  presented decelerated growth rate at the same x-axis coordinate point. As previously stated, when rotation speed was constant, cavitation area was inversely associated to hydrodynamic effect, which had a significant impact on hydrodynamic stiffness  $\Delta K$ . It was obvious that  $\Delta K$  would stop changing while cavitation area was zero, and this was the result of cavitation effect and hydrostatic effect. When increment of  $K_0$  caused by the increasing sealing pressure  $P_o$  was less than reduction in  $\Delta K$ , the total

stiffness  $K$  would undoubtedly decrease, otherwise the rising recovery appeared. The outer diameter pressure  $P_o$  acts on the cavitation effect and hydrostatic pressure at the same time, which caused the total stiffness curve to decrease first and then increase.

$$K = K_0 + \Delta K \tag{21}$$

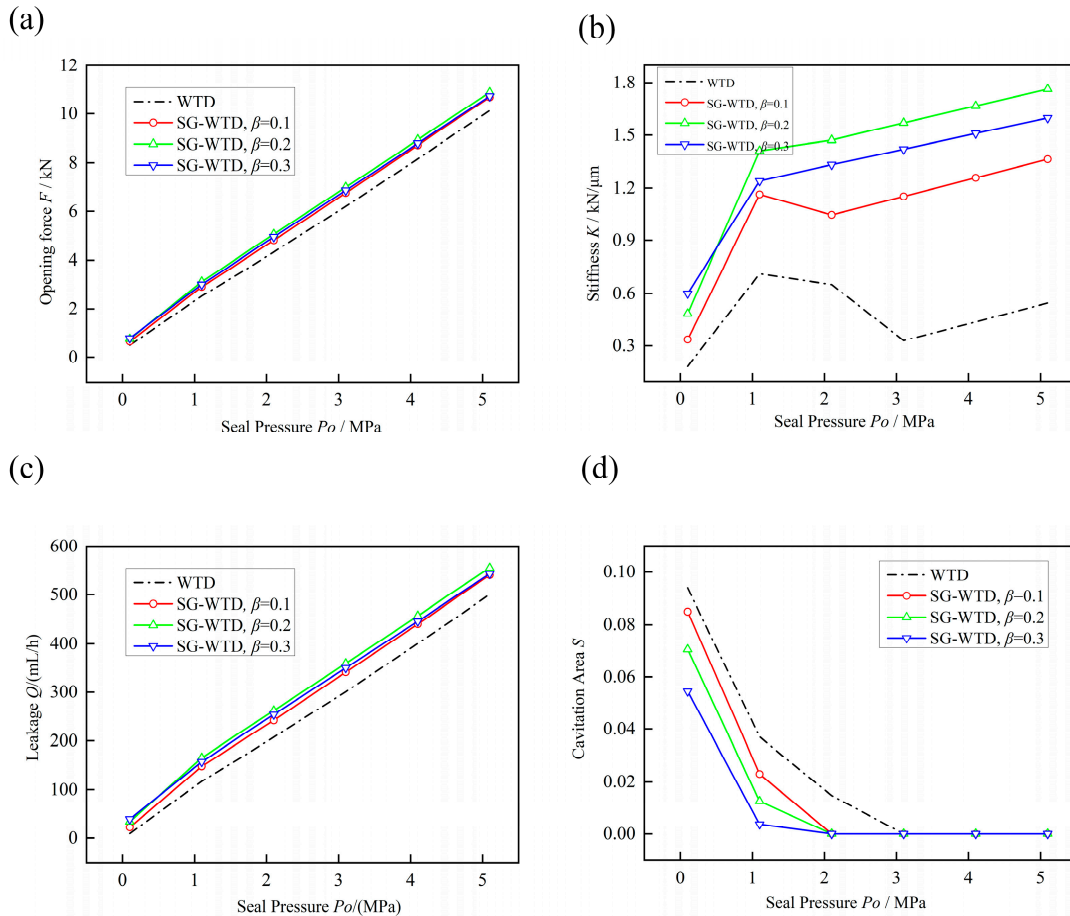


**Figure 5.** Influence of pressure at outer diameter on mechanical performance ( $\alpha = 0.7$ ,  $\lambda = 0.7$ ,  $\omega = 1500$  rpm), (a) opening force, (b) stiffness, (c) leakage, (d) cavitation.

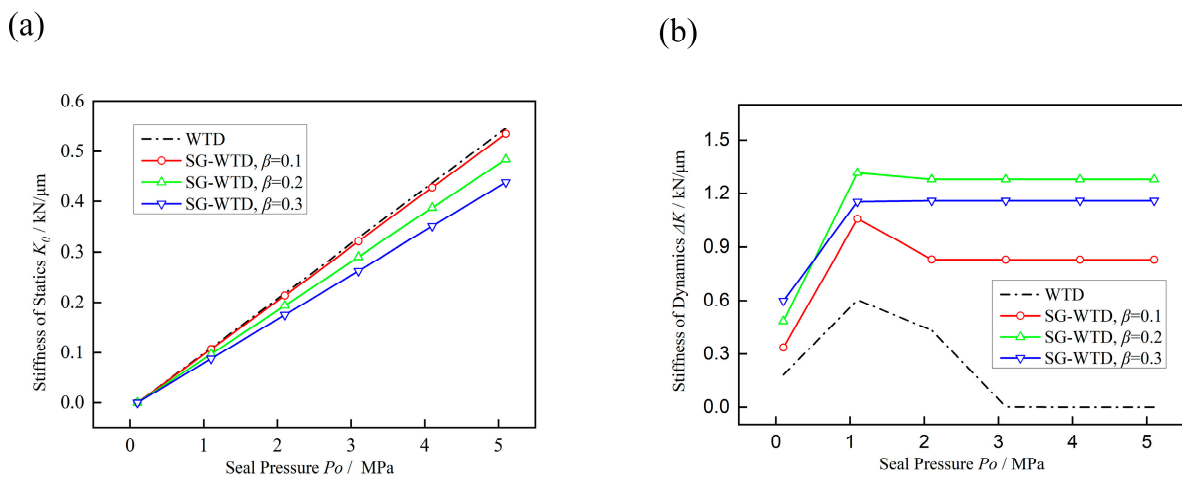


**Figure 6.** Curves of total stiffness, (a) stiffness of statics, (b) stiffness of dynamics.

### 3.3. Influence of Geometric Parameters

The hypothetic settings including the operational condition:  $\omega = 1500$  rpm,  $P_o = 1.1$  MPa, remain constant without specification. Three geometric parameters consisting of  $\alpha$ ,  $\beta$  and  $\lambda$  were selected as variants used to investigate the influence on mechanical performance.

#### 3.3.1. Influence of the Shape of Sinusoidal Pattern $\lambda$

Figure 7 shows the change of seal capacity with increase of  $\beta$  at different values of coefficient  $\lambda$ . The maximum of stiffness and opening force in all curves were by the structure parameters  $\beta = 0.2$ . Therefore, the same optimum value of  $\beta = 0.2$  was applied in this section, and  $\lambda$  was defined as 0.5, 0.7, 0.8, respectively. According to the results, the ratio  $\lambda$  had significant effects on shape of seal in the mating ring, and parameter  $\beta$  primarily decided magnitude of micro-structure observed from angle of view that was perpendicular to the sealing face. Due to obvious difference on the shape of lines, the  $\beta$  value of optimum in the line with  $\lambda = 0.5$  was 0.4 which was twice as much as x-axis coordinate of optimum in other curves. Refer to equations of governing structure, as shown Equations (1) and (2), it was obvious that the angle distance of structural distribution with parameters  $\beta = 0.2$  and  $\lambda = 0.7$  was approximately close to that of the governing parameters  $\beta = 0.4$  and  $\lambda = 0.5$ . If the minor distinction between  $\lambda = 0.7$  and  $\lambda = 0.75$  was neglected, the magnitudes of structures confirmed by  $\beta = 0.2$  and  $\beta = 0.4$  could be treated as equivalent. Even if a slight structural difference occurred, the trough trend did not contradict the key properties of SG-WTD seals.

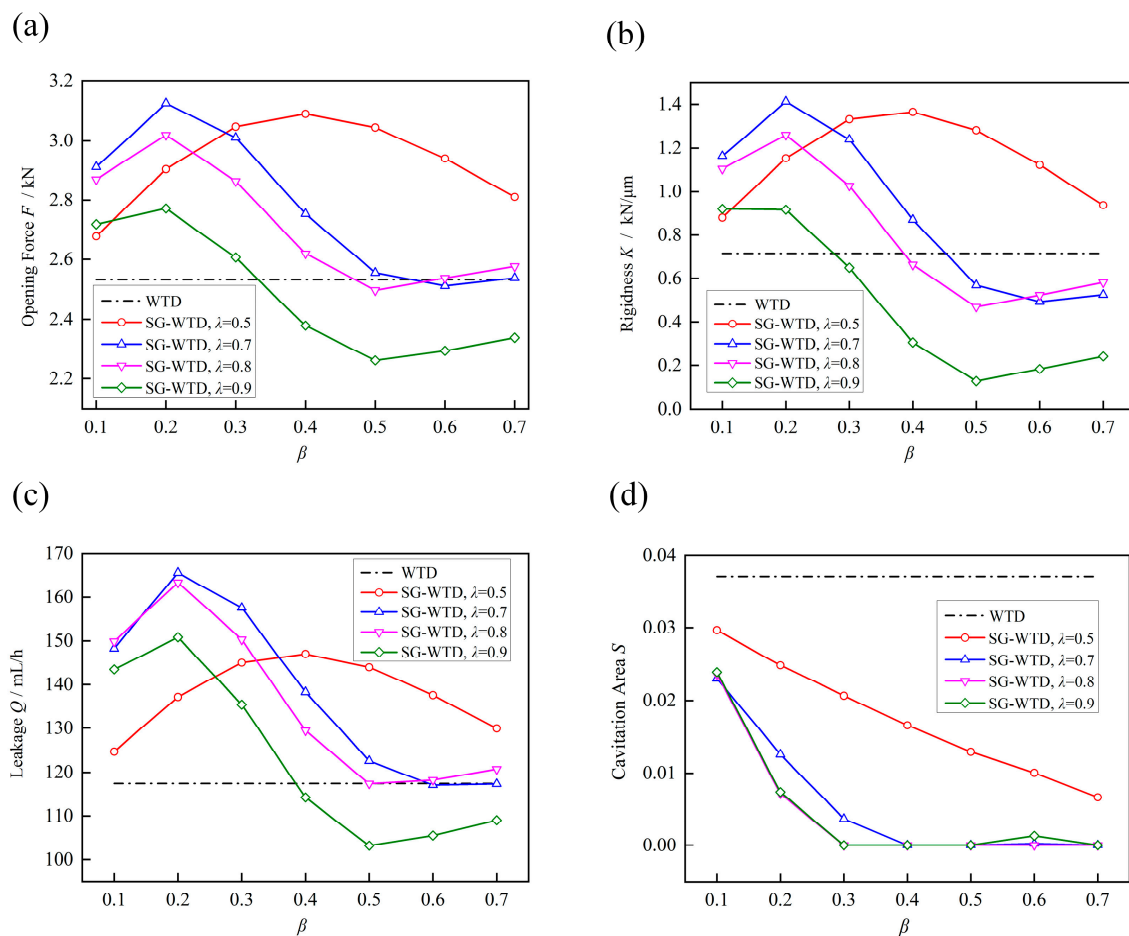


**Figure 7.** Influence of parameter  $\lambda$  on curve of performance ( $\alpha = 0.7$ ), (a) opening force, (b) stiffness, (c) leakage, (d) cavitation.

### 3.3.2. Influence of the Divergence Area Proportion $\alpha$

The influence of ratio  $\beta$  on the mechanical performance such as opening force, stiffness, leakage and cavitation can be obtained in Figure 8 under different values of  $\alpha$ . The most significant characteristic was the existence of an optimum value of  $\beta = 0.2$  at a given operation condition for opening force, stiffness and leakage. When  $\beta$  was larger than 0.5, the hydrodynamic effect would be lower than that of WTD seal. Meanwhile, curves shown in Figure 8 demonstrated that the maximum of performance parameters would be acquired when  $\alpha$  was 0.7. Finally, the significant increase ratios of opening force and rigidity relative to the WTD seal are 23.32% and 98.08%, respectively, and an increase in leakage was unavoidable in the case of structural parameters such as  $\alpha = 0.7$ ,  $\beta = 0.2$  and  $\lambda = 0.2$ . The improvement of sealing performance inevitably led to the increase of leakage, which was acceptable as long as it was within the allowed range. Compared with the WTD seal, the SG-WTD seal obtained smaller cavitation area.

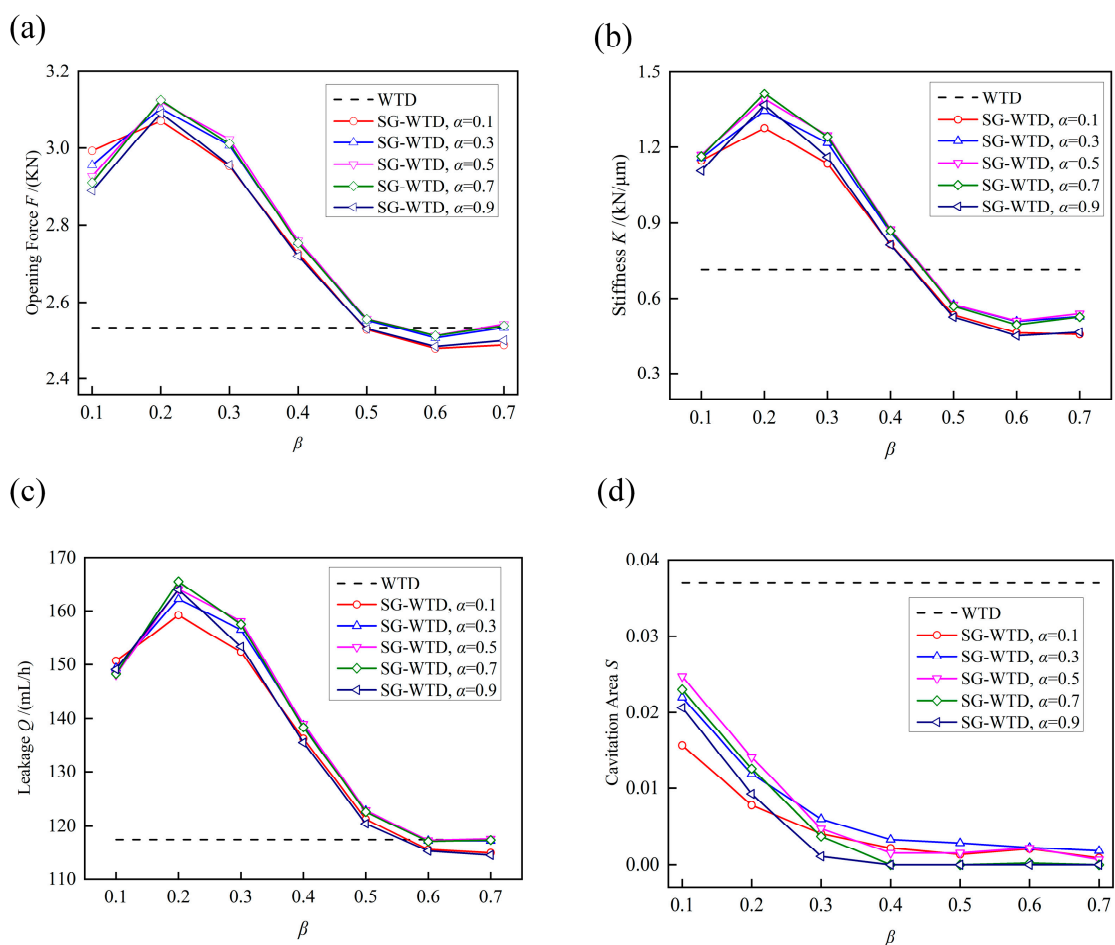


**Figure 8.** Influence of parameter  $\alpha$  on curve of performance ( $\lambda = 0.7$ ), (a) opening force, (b) stiffness, (c) leakage, (d) cavitation.

## 4. Conclusions

In this article, a new type of seal, known as the SG-WTD seal, is introduced, which utilizes a combination of wave-tilt-dam and Spiral Groove structures to enhance the hydrodynamic effect of fluid film. The study presents the results of parametric investigations conducted on the seal, and the main conclusions are drawn. The incorporation of a varying phase with radial coordinates was found to greatly improve the hydrodynamic properties of the sealing surface, resulting in an increase in opening force and rigidity. Specifically, the film rigidity was found to be 98.08% greater than that of the WTD seal, when the structural parameters  $\alpha$ ,  $\beta$ , and  $\lambda$  were set to 0.7, 0.2, and 0.2, respectively. The hydrodynamic effect

of the varying phase structure is dependent on the control parameters, and proper design of these parameters can lead to significant improvements in rigidity. However, it should be noted that an increase in hydrodynamic effect may also result in an increase in the loss of sealing liquid.

**Author Contributions:** Conceptualization, P.Z. and Y.Y.; methodology, T.H.; software, Q.Z.; validation, formal analysis, investigation, T.H., Y.Y. and J.D.; resources, data curation, writing—original draft preparation, writing—review and editing, T.H. and Y.Y.; visualization, supervision, project administration, funding acquisition, T.H. All authors have read and agreed to the published version of the manuscript.

**Funding:** This research was funded by the National Natural Science Foundation of China (No. 52006158).

**Data Availability Statement:** The data presented in this study is openly available.

**Acknowledgments:** The authors appreciate the financial support from the National Natural Science Foundation of China (No. 52006158).

**Conflicts of Interest:** The authors declare no conflict of interest.

## References

1. Cheng, H.S.; Castelli, V. Performance Characteristics of Spiral-Groove and Shrouded Reynolds Step Profiles for High-Speed Non-contacting Gas Seals. *Trans. ASME J. Lubr. Technol.* **1969**, *91*, 60–68. [\[CrossRef\]](#)
2. Wang, Y.M.; Yang, H.Y.; Wang, Y.D. Experimental Investigations and Field Applications of Oil-Film-Lubricated Mechanical Face Seals with Spiral Grooves. *Tribol. Trans.* **2005**, *48*, 589–596. [\[CrossRef\]](#)
3. Wang, Y.M.; Yang, H.Y.; Wang, J.L. Theoretical Analyses and Field Applications of Gas-Film Lubricated Mechanical Face Seals with Herringbone Spiral Grooves. *Tribol. Trans.* **2009**, *52*, 800–806. [\[CrossRef\]](#)
4. Liu, Z.; Liu, Y.; Liu, X.F. Optimization design of main parameters for double spiral grooves face seal. *Sci. China Ser. E-Tech. Sci.* **2007**, *50*, 448–453. [\[CrossRef\]](#)
5. Pennink, H. The Gas Lubricated Spiral Grooved Face Seal in The Process Industry. In Proceedings of the 14th Turbomachinery Symposium, College Station, TX, USA; 1985. [\[CrossRef\]](#)
6. Galenne, E.; Pierre, D.I. Thermo-elasto-hydro-dynamic modeling of hydrostatic seals in reactor coolant pumps. *Tribol. Trans.* **2007**, *50*, 466–476. [\[CrossRef\]](#)
7. Sato, Y.; Ochiai, M. Temperature Distribution Measurement and Internal Flow Visualization in the Lubrication Film of Non-contacting Mechanical Seals. *Tribol. Lett.* **2022**, *70*, 1–14. [\[CrossRef\]](#)
8. Li, Z.; Li, Y.; Cao, H.; Hao, M.; Liu, F.; Meng, D. Investigation of cavitation evolution and hydrodynamic performances of oil film seal with spiral groove. *Tribol. Int.* **2021**, *157*, 106915. [\[CrossRef\]](#)
9. Iny, E.H. A theory of sealing with radial face seals. *Wear* **1971**, *18*, 51–69. [\[CrossRef\]](#)
10. Liu, Y.; Liu, W.; Li, Y.; Liu, X.; Wang, Y. Mechanism of a wavy-tilt-dam mechanical seal under different working conditions. *Tribol. Int.* **2015**, *90*, 43–54. [\[CrossRef\]](#)
11. Lee, S.; Kim, D.; Park, J.Y. Harmonisation of Coolant Flow Pattern with Wake of Stator Vane to Improve Sealing Effectiveness Using a Wave-Shaped Rim Seal. *Energies* **2019**, *12*, 1060. [\[CrossRef\]](#)
12. Key, B.; Dickau, R.; Carlson, B. Mechanical seals with wavy SiC faces for a severe duty NGL/ Crude pipeline application. In Proceedings of the 21st International Pump Users Symposium, Baltimore, MD, USA, 8–11 March 2004. [\[CrossRef\]](#)
13. Liu, W.; Liu, Y.; Zhai, J.J. Three-Dimensional Flow-Heat Coupling Model of a Wavy-Tilt-Dam Mechanical Seal. *Tribol. Trans.* **2013**, *56*, 1146–1155. [\[CrossRef\]](#)
14. Liu, W.; Liu, Y.; Wang, Y.M. Parametric Study on a Wavy-Tilt-Dam Mechanical Face Seal in Reactor Coolant Pumps. *Tribol. Trans.* **2011**, *54*, 878–886. [\[CrossRef\]](#)
15. Liu, W.; Liu, Y.; Huang, W.F. Effect of disturbances on the dynamic performance of a wavy-tilt-dam mechanical seal. *Tribol. Int.* **2013**, *64*, 63–68. [\[CrossRef\]](#)
16. Yu, H.; Huang, W.; Wang, X. Dimple patterns design for different circumstances. *Lubr. Sci.* **2013**, *25*, 67–78. [\[CrossRef\]](#)
17. Bai, S.; Peng, X.; Li, Y. A hydrodynamic laser surface-textured gas mechanical face seal. *Tribol. Lett.* **2010**, *38*, 187–194. [\[CrossRef\]](#)
18. Reynolds, O. On the theory of lubrication and its application to Mr. Beauchamp Tower's experiments including an experimental determination of the viscosity of olive oil. *Philos. Trans. R. Soc. Lond.* **1886**, *A177*, 157–234. [\[CrossRef\]](#)
19. Laratta, A.; Marzulli, P. Cavitation phenomena in lubricated bearings: Computing method and results. *Meccanica* **1972**, *7*, 60. [\[CrossRef\]](#)
20. Li, J.H.; Liu, X.F.; Huang, W.F. A Finite Element Cavitation Algorithm Using Free Mesh for Mechanical Face Seal. *Adv. Mater. Res.* **2011**, *199–200*, 670–677. [\[CrossRef\]](#)
21. Jang, G.H.; Chang, D.I. Analysis of a hydrodynamic herringbone grooved journal bearing considering cavitation. *J. Tribol.* **2000**, *122*, 103–109. [\[CrossRef\]](#)

22. Brewe, D.E.; Jacobson, B.O. The effect of vibration amplitude on vapour cavitation in journal bearings. *Wear* **1987**, *115*, 63–73. [[CrossRef](#)]
23. Hajjam, M.; Bonneau, D. A transient finite element cavitation algorithm with application to radial lip seals. *Tribol. Int.* **2007**, *40*, 1258–1269. [[CrossRef](#)]
24. Kumar, A.; Booker, J.F. A Mass and Energy Conserving Finite Element Lubrication Algorithm. *J. Tribol.* **1994**, *116*, 667–671. [[CrossRef](#)]
25. Grün, J.; Feldmeth, S.; Bauer, F. Multiphase Computational Fluid Dynamics of Rotary Shaft Seals. *Lubricants* **2022**, *10*, 347. [[CrossRef](#)]
26. Booker, J.F.; Huebner, K.H. Application of Finite Element Methods to Lubrication: An Engineering Approach. *J. Lubr. Technol. Trans. ASME* **1972**, *94*, 313–323. [[CrossRef](#)]

**Disclaimer/Publisher’s Note:** The statements, opinions and data contained in all publications are solely those of the individual author(s) and contributor(s) and not of MDPI and/or the editor(s). MDPI and/or the editor(s) disclaim responsibility for any injury to people or property resulting from any ideas, methods, instructions or products referred to in the content.